第 26卷 第 8期
2005年 8月

焊 接 学 报
TRANSACTIONS OF THE CHINA WELDING INSTITUTION

Vol.26 No.8
August 2005

Al_2O_3纤维增强铝基复合材料储能焊接头微观组织分析

翟秋亚， 雷 鸣， 徐锦锋
（西安理工大学 材料科学与工程学院，西安 710048）


翟秋亚

摘 要：应用自制微型储能电阻焊机对 Al_2O_3纤维增强铝基复合材料进行了点焊连接，分析了接头的组织形貌。在储能焊接头中形成了规则的扁平熔核，复合材料基体与熔核金属过渡良好。极短的焊接时间和大的冷却速率使共晶 Si显著细化。细小的共晶 Si颗粒均匀分布于铝基体中，形成与 MMCs不同的基体组织。少量 Al_2O_3 纤维发生了一定程度的破碎，大部分纤维仍保持其原有的形貌特征，随机分布于熔核金属基体中。适当增大电极压力，焊前对复合材料做除氢处理并保持干燥是减小和消除气孔、提高和改善 MMCs储能焊接头质量的有效途径。

关键词：复合材料；Al_2O_3纤维；储能焊；接头组织
中图分类号：TG457.19 文献标识码：A 文章编号：0253-360X(2005)08-65-04

0 序 言

金属基复合材料（MMCs）以其高的比强度、耐磨、耐高温、抗辐射及尺寸稳定性能，在航空、航天、汽车等工业领域有着广泛的应用前景。由于 MMCs中基体金属与增强相之间的物化性能存在较大差异，其焊接难度较大[1]。目前，关于 MMCs连接方法的研究主要有激光焊[2,3]、氩弧焊[4]、电阻焊[5,6]、摩擦焊[7]和扩散（钎）焊[8~10]。熔化焊焊缝容易产生增强相的熔化、偏聚，相间难熔合及气孔等缺陷；固态焊需要较大的机械能，而且焊接变形量亦较大；扩散焊和钎焊去膜难度大，结合界面易产生夹杂和微裂纹，直接影响接头的使用性能。硬规范电容储能焊具有瞬间放电和快速连接的特点，熔核冷却速率大，达 10^6 K/s之多，易获得组织细小、致密的连接接头[11~13]。并且熔核在电极压力下凝固，能够在破碎和挤出氧化膜的同时，有效地减小连接区内的孔洞缺陷。因此，储能焊在金属材料连接领域具有一定的优越性。然而，有关 MMCs储能焊的研究报道尚不多见。文中采用自行研制的微型储能电阻焊机对 Al_2O_3纤维增强铝基复合材料进行了储能焊连接，分析了接头的结构和组织特征，探讨了熔核中气孔的形成机制。

收稿日期：2004-08-24

1 试验方法

1.1 试样制备

Al_2O_3纤维增强铝基复合材料由高压低速金属型铸造法制备而成。Al_2O_3纤维的体积分数为 9%，直径约 4 μm，长度在 40 ~ 200 μm。金属基体（ADC12）的成分为（质量分数，%）：10.8Si，2.5Cu，其余为 Al。焊接试样的尺寸为 10 mm × 5 mm × 0.2 mm的板材，系线切割加工而成。纤维的排布方向与试样的厚度方向平行而与长度方向呈一定角度随机分布。

1.2 储能焊连接

试样经 1 200目金刚砂纸打磨、丙酮清洗后，装配成如图 1所示的搭接接头。在自制微型电容储能电阻焊机上进行点焊连接。焊接参数为：电压 U = 80 ~120 V，电容 C = 2500 ~4000 μF，电极压力 F = 15 ~20N。焊接能量、焊接电压和电容之间的函数关系为：$W = CU^2/2$，因此，焊接能量 W = 8.0 ~28.8 J。采用 V-422型示波器监控电容放（充）电压特性。

1.3 接头组织观察

焊接接头样品经用树脂镶嵌、抛光和 0.5%氢氟酸水溶液浸蚀后，在 XJG-05型光学显微镜和 ARMRAY-1000B型扫描电镜上观测和分析接头的组织形态。

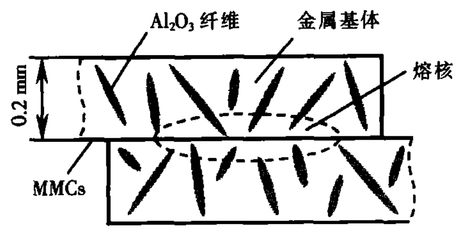

图 1 MMCs储能焊搭接接头示意图
Fig. 1 Schematic diagram of lap joint of condenser discharge spot welding for MMCs

2 结果与讨论

2.1 MMCs储能焊接头形貌

图 2a为经过浸蚀的 MMCs点焊接头整体形貌。从中看出,在点焊接头中形成了规则的扁平熔核,熔核厚度约占接头厚度的 1/2~2/3,其厚宽比约为 1:(3~5)。图 2b为图 2a的局部放大。由于该图未经浸蚀,因此,可从中清晰地观察和分析接头熔(焊)合状况、接头中 Al_2O_3 纤维形貌及分布特征。由图 2b可见,经历焊接过程,焊区中少量的 Al_2O_3 纤维部分发生了熔断和破碎,呈粒状及短条状分布在熔核之中;大部分纤维仍保持着其原有的形貌特征,经由母材横穿熔合区而直接插入熔核区。可见,储能焊可实现MMCs的连接,熔核与 MMCs间熔合良好,熔核组织细小均匀,未出现明显的宏观偏析。

2.2 MMCs 熔核界面组织特征

图 3a为未经浸蚀的MMCs 熔核结合界面的组织形貌。在界面母材一侧(热影响区),MMCs基体组织没有发生明显的改变,其中粗大的针状共晶 Si清晰可见,增强相 Al_2O_3 纤维随机地分布于金属基体之中。熔核中心区域的 Al_2O_3 纤维仍保持完整的几何形状,但在基体中呈网络状分布的共晶 Si则不复存在。MMCs基体与熔核金属过渡良好,除增强相纤维之外,共晶 Si的形态由 MMCs基体中粗大的针状经由熔合区逐渐向熔核中的粒状共晶 Si过渡。图 3b为经过浸蚀的图 3a的局部放大。从中可以看出,在 MMCs 熔核结合界面处共晶 Si明显熔断、破碎,失去了其原始的针片状形态。在熔核区及由熔核向MMCs过渡的熔合区中,共晶 Si均呈细小颗粒弥散分布于(Al)基体中,而且过渡区组织要比熔核区略显粗大。

2.3 熔核结晶动力学分析

Al_2O_3纤维尺寸大,熔点高,具有一定的刚性,在焊接过程中,具有较强的承受电极压力和热冲击

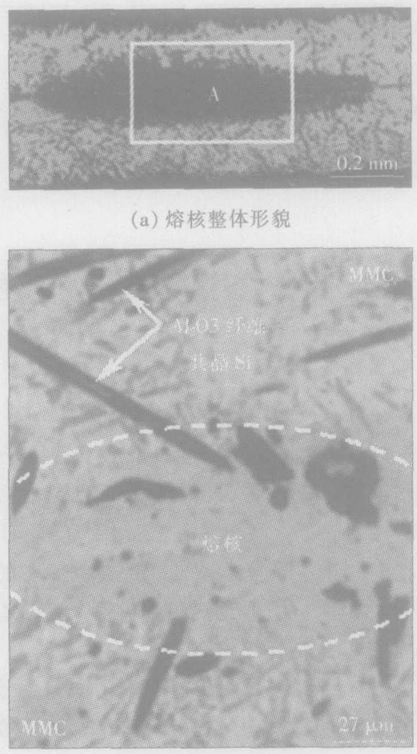

(a) 熔核整体形貌

(b) A区的局部放大

图 2 MMCs储能焊熔核整体形貌
Fig. 2 Microstructure morphology of whole nnugget by condenser discharge spot welding

作用的能力。硬规范储能焊接过程对焊接区 Al_2O_3 纤维的分布状态及尺度无太大的影响。相比之下,共晶 Si的形态、分布和尺寸则受之影响甚大。尽管Si晶体熔点高,但共晶 Si尺寸小,比表面积大,具有较高的界面能。而且 Si原子在(Al)中有一定的固溶度。当基体金属熔化时,Si原子将通过 Si/液态Al界面的原子迁移而溶解于 Al液之中。熔核中心温度高、原子迁移时间相对稍长,因而 Si晶体的溶解充分。而界面处温度较低,共晶 Si的熔化分解不能充分进行,因而在界面基体中能够明显地观察破碎的或开花状共晶 Si,这些共晶 Si实际上是业已部分熔化的针状共晶 Si的残迹,如图 3b中椭圆区内所示。

电容放电结束后,由于 Cu电极和周围基体的快速吸热,熔核处于较大的过冷状态。Si晶体的形核率高,生长速度快,(Al)和 Si相耦合生长的机制被打破,因而形成(Al)基体上分布着大量细碎的点状共晶 Si的组织结构。由于共晶 Si的细化使基体中晶界增多,对浸蚀液的敏感性增强,浸蚀速度变快,因而在光学显微镜下呈现出较深的颜色,如图3b所示。图中弥散分布的 Si颗粒依稀可辨。这种组织结构与 MMCs中的基体组织有着显著的不同。

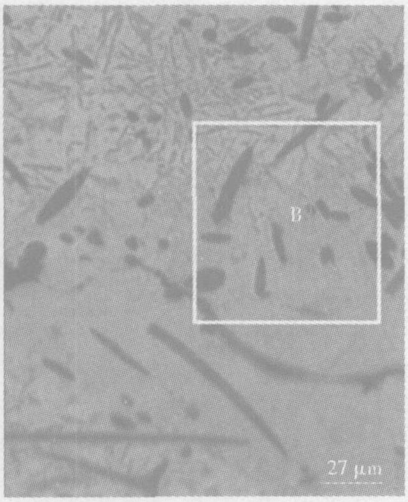

(a) 熔合区形貌

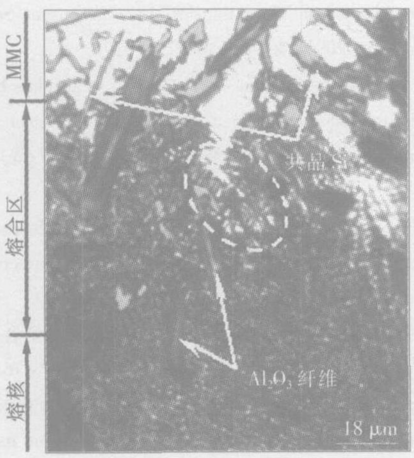

(b) B区的局部放大

图 3　MMCs储能焊熔合区组织特征

Fig. 3　Microstructural characteristics of bond area by condenser discharge spot welding

另外,在复合材料的制备过程中,由于存在晶体学共格对应关系,共晶 Si通常会依附 Al_2O_3 纤维的表面形核生长。然而,由于储能焊持续时间极短(毫秒级),Si晶体的生长尺度非常有限,加之熔核冷却速率很大,形核率高,Si原子的扩散受到抑制。因此,熔核中共晶 Si依附 Al_2O_3 纤维/液相界面形核生长行为在一定程度上受到抑制,形成了细小均匀的熔核基体组织。

2.4　气孔的形成机制

试验发现,气孔是 Al基复合材料储能焊过程中最为常见的焊接缺陷。气孔主要产生于 Al_2O_3 纤维的端部,外形不甚规则,具有反应性气孔的特征,如图 4中箭头所示。气孔的产生主要与以下三种因素有关:电极压力、Al_2O_3 纤维表面的挥发物及 MMCs中的含氢量。

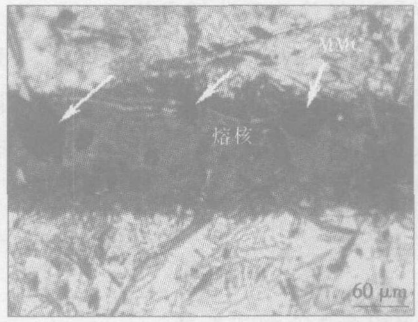

图 4　储能焊熔核中气孔的形貌

Fig. 4　Pore morphology in nugget by condenser discharge spot welding

2.4.1　电极压力

电极压力对气孔的形成具有显著的影响。金属熔体中形成的稳定气泡,其内部压力 p_i 可由下式表示

$$p_i = p_\sigma + p_a + p_f \tag{1}$$

式中:$p_\sigma = 2\sigma/r$为熔体表面张力引起的附加压力;σ为表面张力,r为气泡的半径;p_a为熔体对气泡产生的静压力;p_f为电极压力。

在储能焊条件下,熔核尺寸微小,熔体的静压力可忽略不计。因此,式(1)可简化为

$$p_i = 2\sigma/r + p_f\ 。 \tag{2}$$

假设半径为 r_0 的显微气泡在焊接过程中从温度 T_0加热至温度 T,其半径变为 r。则由理想气体定理可得下列关系式

$$nRT_0 = p_0V_0 = 4(2\sigma/r_0 + p_f)\pi r_0^3/3, \tag{3}$$

$$nRT_0 = pV = 4(2\sigma/r + p_f)\pi r^3/3, \tag{4}$$

式中:n为气泡内气体摩尔数;R为气体常数;p_0和 V_0分别为温度 T_0下的气泡压力和体积;p和 V分别为温度 T下的气泡压力和体积。

联立式(3)和式(4),可得下式

$$p_f = 2\sigma(r_0^2T - r^2T_0)/(r^3T_0 - r_0^3T)。 \tag{5}$$

如果考虑 m 个半径为 r_0 的气泡合并为一个半径为 r的大气泡的情况,易得

$$p_f = 2\sigma(m r_0^2T - r^2T_0)/(r^3T_0 - m r_0^3T)\ 。 \tag{6}$$

通过测定焊件原材料中的显微气泡半径 r_0、熔核区平均显微气泡的数量 m,气泡长大的有效温度范围及合金的表面张力 σ,即可应用式(5)和式(6)定量分析电极压力与气泡长大和合并的相关规律。

随电极压力增大,熔核中压力增大,气泡难以形核长大。因此,在保证起弧熔化形成熔核的前提下,电极压力应取上限值,以减小和消除气孔的产生。

2.4.2 Al_2O_3纤维表面的挥发物

在采用高压低速金属型铸造法制备MMCs的过程中,通常使用 Al_2O_3 纤维和有机粘结剂组成的混合料来制备预制体。在MMCs成形过程中,如果有机物去除不彻底,会造成微量有机物残留于 Al_2O_3 纤维表面,熔化焊时成为熔核中气孔的发源地。

2.4.3 MMCs基体的含氢量

氢在铝液中具有一定的溶解度,基体金属本身的含气量大是形成熔核气孔的原因之一。另外,附着在焊件表面的潮气在焊接时也会增加吸氢的机会而导致气孔的产生。因此,除采用合理的焊接工艺外,焊前对复合材料做适当的除氢处理并保持干燥是减小和消除气孔、提高和改善MMCs储能焊接头质量的有效途径。

3 结 论

(1)采用微型储能焊机可实现 Al_2O_3 纤维增强铝基复合材料的焊接。在储能焊接头中形成了规则的扁平熔核,MMCs基体与熔核金属过渡良好,熔核中除少量 Al_2O_3 纤维发生一定程度的破碎之外,大部分纤维仍保持着其原有的形貌特征,经由母材横穿熔合区而直接插入熔核区,随机分布于焊接接头之中。

(2)在储能焊条件下,极短的焊接时间和大的冷却速率使共晶Si显著细化。细小的共晶Si颗粒均匀弥散的分布于金属基体中,形成与MMCs不同的熔核组织。

(3)适当增大电极压力,焊前对复合材料进行除氢处理并保持干燥是减小和消除气孔,提高和改善MMCs储能焊接头质量的有效途径。

参考文献:

[1] Ageorges C, Ye L, Hou M. Advances in fusion bonding techniques for joining thermoplastic matrix composites: a review[J]. Composites Part A, 2001, 32(6): 839-857.

[2] Liu Liming, Zhu Meili, Xu Weiping, *et al*. Laser welding mechanism and parameters of aluminum matrix composite SiCw/6061Al[J]. Transaction of the China Welding Institution, 2001, 22(4): 13-16.
刘黎明, 祝美丽, 徐卫平, 等. 铝基复合材料SiCw/6061Al的激光焊接[J], 焊接学报, 2001, 22(4): 13-16.

[3] Niu Jitai, Zhang Deku, Ji Guojuan. Effect of parameters on microstructure of joint in laser beam welding for SiCp/6063 composite[J]. Trans Nonferrous Met Soc China, 2003, 13(2): 289-293.

[4] Lean P P, Gil L, Ureña A. Dissimilar welds between unreinforced AA6082 and AA6092/SiC/25p composite by pulsed-MIG arc welding using unreinforced filler alloys(Al-5Mg and Al-5Si)[J]. Journal of Materials Processing Technology, 2003, 143-144: 846-850.

[5] Ageorges C, Ye L. Resistance welding of thermosetting composite/thermoplastic composite joints[J]. Composites Part A, 2001, 32(11): 1603-1612.

[6] Ageorges C, Ye L, Hou M. Experimental investigation of the resistance welding of thermoplastic-matrix composites. Part Ⅰ: heating element and heat transfer[J]. Composites Science and Technology, 2000, 60(7): 1027-1039.

[7] Wert J A. Microstructures of friction stir weld joints between an aluminium-base metal matrix composite and a monolithic aluminium alloy[J]. Scripta Materialia, 2003, 49(6): 607-612.

[8] Lu Shixiong, Yu Zhishui, Xu Zhiwu, *et al*. Fluxless pressure soldering for SiCw/6061Al composites[J]. Transactions of the China Welding Institution, 2001, 22(4): 73-76.
吕世雄, 于治水, 许志武, 等. SiCw/6061Al复合材料无钎剂加压钎焊[J]. 焊接学报, 2001, 22(4): 73-76.

[9] Zhang X P, Quan G F, Wei W. Preliminary investigation on joining performance of SiCp-reinforced aluminium metal matrix composite(Al/SiCp-MMC) by vacuum brazing[J]. Composites Part A, 1999, 30(6): 823-827.

[10] Liu Liming, Zhu Meili, Pan Longxiu, *et al*. Studying of micro-bonding in diffusion welding joint for composite[J]. Materials Science and Engineering, 2001, A315(1-2): 103-107.

[11] Xu Jinfeng, Zhai Qiuya, Yuan Sen. Energy-storage welding connection characteristics of AZ91D magnesium alloy rapid solidification ribbons[J]. Journal of Materials Science and Technology, 2004, 20(4): 431-434.

[12] Ellis M B D. Joining of aluminium based metal matrix composites[J]. International Materials Reviews, 1996, 41(2): 1-58.

[13] Xu Jinfeng, Zhai Qiuya, Jiang Yong. Energy-storage welding connection characteristics of rapidly solidified Cu-Co alloy foils[J]. Trans Nonferrous Met Soc China, 2004, 14(4): 785-789.

作者简介: 翟秋亚, 女, 1963年9月出生, 副教授, 硕士。主要从事先进材料及其焊接方面的研究, 发表论文40余篇。

Email: xu-zhai@xaut.edu.cn

formance of coating sprayed by High Velocity Oxygen/Air Fuel spray system, which is mostly dependent on the flame temperature and velocity accelerated by convergent-divergent nozzle. Gas characteristics of inlet, throat and outlet of the nozzle are calculated. Characteristic diameter and inner shape of the nozzle is designed according to aerodynamics. The results show that the velocity of the flame reaches supersonic while oxygen and air is used as combustion-supporting gas respectively. At the same time, the pressure of the nozzle outlet is less than the ambient pressure, which is advantageous to powder feeding. Flame velocity can be continuously adjusted from 1 400 to 2 150 m/s, while flame temperature is 1 400 ~ 2 600 ℃. The adjustable flame can meet the requirement of spraying coating for metal, alloy and ceramics.

Key words: convergent-divergent nozzle; particle velocity; particle temperature; coating

Microstructure analysis on capacitor discharge welded Al_2O_3 fiber reinforced Al-matrix composites joint ZHAI Qiu-ya, LEI Ming, XU Jin-feng (School of Materials Science and Engineering, Xi'an University of Technology, Xi'an 710048, China). p65 – 68

Abstract: The resistance spot welding of the Al_2O_3 fiber reinforced Al-matrix composites (MMCs) was conducted using a micro-type capacitor discharge welding machine and the microstructural morphology of the joint was investigated. The results showed that a regular, flat nugget was formed in the joint and the microstructural transition from nugget to matrix was rather well. Due to the very short welding time and high cooling rate, the eutectic Si was refined remarkably. The tiny eutectic Si particles distributed uniformly in the Al-matrix, resulting in microstructure different from the MMCs. Small quantity of Al_2O_3 fibers were broken down to some extent, while most of them remained their original morphology, distributing in the nugget matrix randomly. It was considered an effective way to eliminate the porosity and improve the joint quality, i.e. increasing electrode pressure properly, removing hydrogen from MMCs and holding the MMCs dry.

Key words: MMCs; Al_2O_3 fiber; capacitor discharge welding; joint microstructure

Influence of welding thermal cycle on toughness and microstructure in grain-coarsening region of X80 pipeline steel XU Xue-li, XIN Xi-xian, SHI Kai, ZHOU Yong (Department of Materials Science and Engineering, Xi'an Shiyou University, Xi'an 710065, China). p69 – 72

Abstract: The influence of welding thermal cycle on toughness and microstructure in grain-coarsening region in the heat affected zone (HAZ) of X 80 pipeline steel was investigated by weld thermal simulation technique, metallography, transmission electron microscopy (TEM), the instrumented Charpy impact toughness test and fracture toughness test. The results showed that there were different microstructures in the simulated grain-coarsening region of X80 pipeline steel under six different weld thermal cycle conditions. When the thermal cycling parameters were small, the microstructure of grain-coarsening region was primarily lower bainite and lath martensite, and when the thermal cycling parameters increased, it was mainly granular bainite. The structural morphology of M-A islands changed from thin and short bars to large long bars or large piece-like, and distributed in the grains instead of on the grain boundary. At the same time, the number of the M-A islands increased and the toughness got worse.

Key words: pipeline steels; welding thermal cycle; grain-coarsening region; toughness; microstructure

Research on vacuum electron beam welding of 45CrNiMoVA steel DOU Zheng-ping, XIE Zhi-qiang, PEI Qiu-sheng, JIANG Yun-bo (Chinese Academy of Engineering and Physics, Mianyang 621900, Sichuan, China). p73 – 76

Abstract: The electron beam welding technology of 45CrNiMoVA steel was analyzed and discussed in the paper, and the microstructure profile and mechanical properties of weld were examined by metallography, scanning electron microscope and fracture analysis, etc. Then, we analyzed the factors causing cracks and methods to prevent them, and chose the reasonable process weld depth being 20mm. The results showed the weld of 45CrNiMoVA steel welded by electron beam had demonstrable superiorities— good mechanical properties and high strength, well results were got by colored detecting on surface, and X-ray detecting carried on the weld.

Key words: 45CrNiMoVA steel; electron beam welding; crack control; microstructure; mechanical property

Study on automatic welding process of curved seam with five welding guns HAN Hong-biao[1], JIA Xian-zhao[1], CUI Qi[2], LI Ji-shun[1] (1. Henan Key Laboratory of Advanced Manufacturing Technology, Henan University of Science and Technology, Luoyang 471003, China; 2. Yituo (Luoyang) Building Machinery Corp., Ltd, Luoyang 471003, China). p77 – 80

Abstract: There are a lot of welds between cooling tubes and mainstream tubes in radiator. These welds are plane curve with complicated shape. The plate is thin and the welding groove size is non-uniform. These result in many welding defects. To achieve automatic welding of these welds, an automatic welding machine and automatic welding process were developed. A numerical control system controlled five welding guns to move along the welding seam simultaneously. Five welding machines were controlled to work synchronously. Different welding conditions and moving tracks were adopted in different weld segments which had different welding groove shape and size. Therefore, five welds could be achieved at the same time. The quality of welds was guaranteed and the production efficiency was raised. The machine and the automatic welding process have been used in mass production of radiators.

Key words: automatic welding; process; curved welding seam